Selection Studies for the Search of $B_s^0 \to \tau^+\tau^-$ Decay at LHCb using Run 3 Data

Author: Lai Gui

Supervisor: Rita De Sousa Ataíde Da Silva

Responsible Professor: Prof. Frédéric Blanc

Laboratoire de Physique des Hautes Énergies

École Polytechnique Fédérale de Lausanne

January 16, 2026

Travail de Spécialisation pour Master en physique (TSM)

PHYS-597

Contents

Abstract

This report details a selection study performed for the search of the rare decay $B_s^0 \to \tau^+\tau^-$ using data collected by the LHCb experiment during its Run 3. The project focuses on finalising a Boosted Decision Tree (BDT) classifier to suppress combinatorial background and conducting a preliminary investigation into a specific physics background channel. Using data from 2024 (Blocks 7 & 8) and Monte-Carlo (MC) generated signal events, it is demonstrated that the updated BDT achieved an AUC score of 0.957 and significantly suppressed combinatorial background. Along with the $\Delta m_{B_s{}^0}$ cut, an overall efficiency of 0.46% for the Same Sign (SS) data is reached while keeping 60.00% of the signal events. Furthermore, a preliminary study on the physics background $B^0 \to (D^- \to \pi^-\pi^+\pi^-\pi^0)\,\pi^+\pi^-\pi^+$ is performed. Using the selection strategies of the $\Delta m_{B_s{}^0}$ cut, the BDT trained on SS data, as well as the newly discovered $m_{6\pi}$ cut, an overall efficiency of 22.20% is reached while maintaining 64.21% of the signal events. Further study could potentially design a BDT using the MC tuples of this physics background. Similar studies can also be performed on other physics background channels.

1 Introduction

The search for rare decays of B mesons provides a precision test of the Standard Model (SM) of particle physics. Deviations from theoretical predictions in these channels can serve as sensitive indicators of New Physics (NP). This project focuses on the search for the $B_s^0 \to \tau^+\tau^-$ decay using the improved capabilities of the LHCb detector in Run 3.

1.1 LHCb Experiment: Run 3

LHCb (Large Hadron Collider beauty experiment) is one of the four main experiments at the Large Hadron Collider (LHC) at CERN, as shown in Fig. 1. It records data from proton–proton collision events using a series of high-precision detectors to reconstruct the underlying physical processes occurring at the interaction point. By probing matter and fundamental forces at extremely small distance scales and high energies (conditions similar to those just after the Big Bang), LHCb contributes to our understanding of the structure and evolution of the universe.

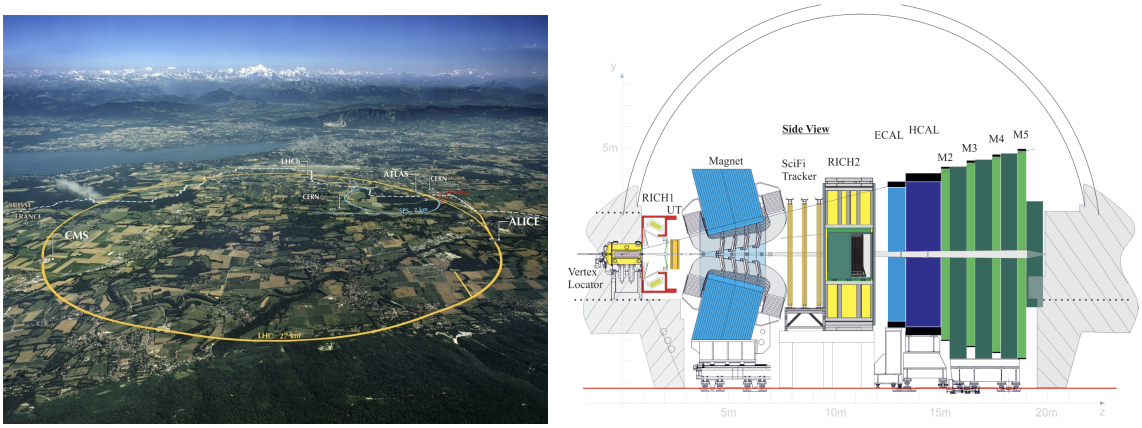

Figure 1: Left: Aerial view of the LHC and its four major experiments [1]. Right: Schematic layout of the LHCb detector [2].

The LHCb detector is a single-arm forward spectrometer covering the pseudorapidity range $2 < \eta < 5$, specifically designed for the study of particles containing b or c quarks. At the LHC energies, $b\bar{b}$ pairs are predominantly produced in the forward directions due to the collision kinematics of the constituent partons (gluon fusion). This forward geometry allows LHCb to capture approximately 25% of the total heavy-flavour production cross-section despite covering only a small fraction of the solid angle [3].

Run 3, which began data taking from 2022, features a significant upgrade to the detector readout and trigger system. The hardware-based Level-0 trigger has been removed and replaced by a full-software trigger system (HLT1 & HLT2) running on GPUs, allowing the detector to read out at the full LHC bunch-crossing rate of 30 MHz [4]. This allows for data collection at a significantly higher instantaneous luminosity of $2 \times 10^{33}\,\mathrm{cm}^{-2}\mathrm{s}^{-1}$ [5]. The increased center-of-mass energy, rising from 13 TeV in Run 2 to 13.6 TeV in Run 3, results in a roughly linear increase in the $b\bar{b}$ production cross-section. This higher luminosity and energy allow more abundant B-meson production, which is critical for rare decay searches.

1.2 $B_s^0 \to \tau^+\tau^-$: Theoretical Context

The decay $B_s^0 \to \tau^+\tau^-$ is a Flavour Changing Neutral Current (FCNC) process. In the Standard Model, tree-level FCNC processes are forbidden. Consequently, this decay can only proceed through higher-order electroweak diagrams, specifically loop processes, such as the W/Z penguin diagram, or the box diagram involving a top quark, W bosons and a neutrino, as featured in Fig. 2.

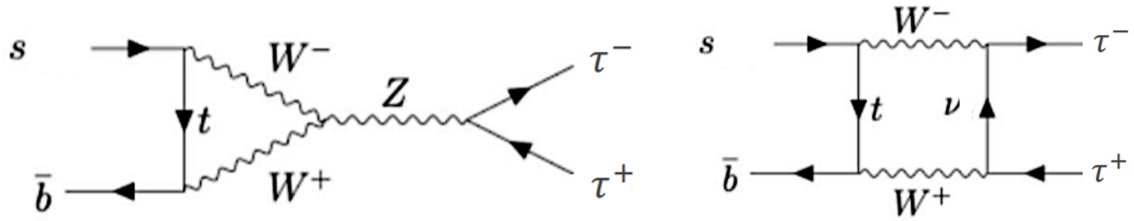

Figure 2: Feynman diagrams contributing to the $B_s^0 \to \tau^+\tau^-$ decay in the Standard Model, illustrating the penguin (left) and box (right) loop processes.

The decay is heavily suppressed in the SM due to two main factors: the GIM suppression in the loop diagrams and the helicity suppression. The SM branching ratio is predicted to be

$$\mathcal{B}(B_s^0 \to \tau^+\tau^-)_{\text{SM}} = (7.73 \pm 0.49) \times 10^{-7}. \tag{1}$$

This prediction is relatively precise due to recent improvements in Lattice QCD calculations of the B_s decay constant f_{B_s} and accurate measurements of CKM matrix elements [6]. This clean theoretical baseline makes this channel highly attractive; any significant experimental deviation from the SM prediction would provide compelling evidence for beyond-the-SM (BSM) dynamics.

1.3 Previous Measurement on Run 1 Data

A search for this decay was previously performed by the LHCb collaboration using Run 1 data. A dataset corresponding to an integrated luminosity of 3 fb^{-1} [7] was utilised for the purpose of the study. The approach involved reconstructing the τ leptons through their decay into $\tau^- \to \pi^-\pi^+\pi^-\nu_\tau$.

The primary challenge faced by this study was the presence of at least two neutrinos in the final state (one from each τ). This results in missing energy and momentum, preventing the full reconstruction of the B_s^0 invariant mass peak, which is the standard discriminant in B-physics. Additionally, the broad kinematic distributions make it difficult to separate the signal from the dominant combinatorial background and other partially reconstructed B-decays.

The Run 1 analysis established an upper limit of $\mathcal{B}(B_s^0 \to \tau^+\tau^-) < 6.8 \times 10^{-3}$ (at 95% CL) [7], which is still orders of magnitude above the SM prediction.

1.4 Aim of This Project

The primary aim of this project is to perform selection studies using part of the LHCb Run 3 data to improve the suppression of the backgrounds involved in the search for this rare decay. The specific objectives involve:

- **Finalising the BDT:** To optimise a Boosted Decision Tree (BDT) classifier designed to suppress the combinatorial background.

- **Physics Background Study:** To conduct a preliminary study at a specific physics background channel, $B^0 \to D^- 3\pi$, that mimics the signal topology .

2 Data and Signal Topology

2.1 Data Size and Expected Events

The analysis is performed on a MC Signal sample, a MC Physics background sample (each with 2M events generated), and a subset of the Run 3 data collected in 2024, specifically "Blocks 7 & 8", corresponding to an integrated luminosity of 1.172 fb^{-1}. The total 2024 data corresponds to 9.56 fb^{-1}. The initial numbers of events that pass the HLT2 selection for each of the data samples used are detailed in Tab. 1.

Table 1: Initial number of events in the data samples used for this analysis.

Sample Type	**Description**	**Initial Number**
MC Signal	Simulated $B_s^0 \to \tau^+\tau^- \to (\pi^+\pi^-\pi^+\bar{\nu}_\tau)(\pi^-\pi^+\pi^-\nu_\tau)$	4,772
MC Physics Bkg.	Simulated $B^0 \to (D^- \to \pi^-\pi^+\pi^-\pi^0)\,\pi^+\pi^-\pi^+$	3,104
SS Data	Same-Sign ($\tau^\pm\tau^\pm$) Events (Blocks 7 & 8)	8,481,222
OS Data	Opposite-Sign ($\tau^+\tau^-$) Events (Blocks 7 & 8)	12,963,547

The expected number of signal events is calculated based on the $b\bar{b}$ production cross-section of 1.543×10^{11} fb [8] (scaled linearly from 13 TeV to 13.6 TeV), the fragmentation fraction $f_s \approx 10.5\%$ [9] and the HLT2 efficiency (1.7%). The results are summarised in Tab. 2.

Table 2: Estimated number of signal events produced and selected after HLT2.

Data Sample	**Signal Produced**	**Signal after HLT2**
Block 7 & 8	133.08	2.26
2024 Full Year	1272.25	21.63

For the analysed sample (Blocks 7 & 8), we expect only **2.26 events**. This low yield implies that this specific subsample is only capable for establishing selection limits rather than observation. However, the HLT2 signal efficiency is expected to improve in 2025, which will further increase the yield in future datasets.

2.2 Signal Signature

The signal process is $B_s^0 \to \tau^+\tau^-$, with both τ leptons decaying hadronically into three charged pions and a neutrino ($\tau^- \to \pi^-\pi^+\pi^-\nu_\tau$). This results in a final state of six charged pions (6π) and two missing neutrinos.

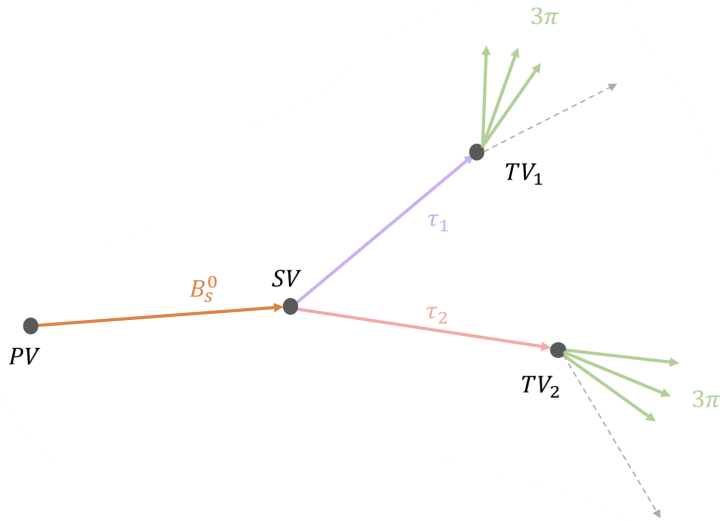

Figure 3: Schematic diagram of decay cascade $B_s^0 \to \tau^+\tau^- \to (\pi^+\pi^-\pi^+\bar{\nu}_\tau)(\pi^-\pi^+\pi^-\nu_\tau)$.

The 3-prong hadronic decay ($\sim 9.31\%$) is chosen over leptonic decays for its distinct topological advantages. The 3-particle vertex acts as a geometric constraint, which is crucial for separating the τ vertices (TV) from the primary interaction vertex (PV) and the B_s^0 decay vertex (SV). Furthermore, the decay proceeds largely through intermediate resonances $\tau^- \to a_1(1260)^-\nu_\tau \to \rho^0(770)\pi^-\nu_\tau$, providing kinematic constraints used in the selection.

2.3 Backgrounds

The analysis deals with two primary sources of background:

1. **Combinatorial Background:** Random combinations of tracks that accidentally satisfy the selection criteria. We use Same-Sign (SS) data (e.g., $\tau^\pm\tau^\pm$) as a data-driven proxy for this background.

2. **Physics Background:** Specific decay channels mimicking the topology of the signal, such as $B_s^0 \to D_s^- D_s^+$, after which each of the $D_s^\pm$ produces 3π. These channels have similar kinematic and isolation characteristics as the signal signature, hence are more difficult to identify compared to the combinatorial background.

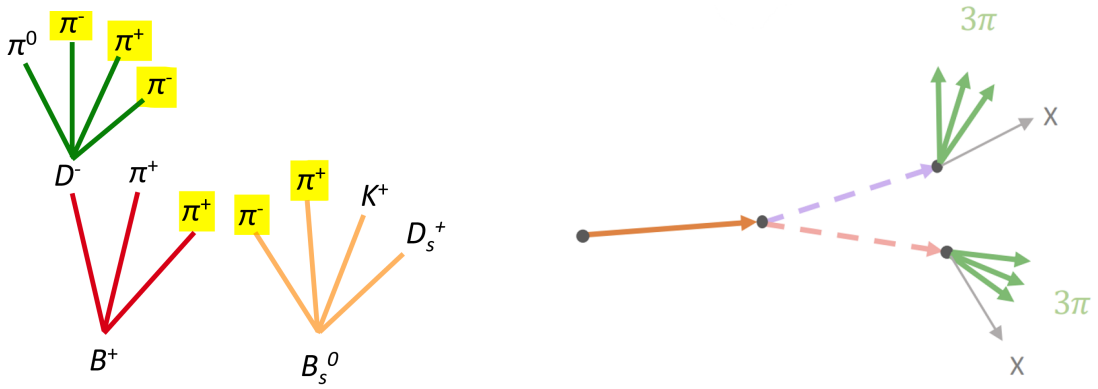

Figure 4: Schematic diagram of Combinatorial Background (left), with random tracks being identified as signal; and Physics Background (right) events.

3 Analysis: Combinatorial Background

3.1 $\Delta m_{B_s^0}$ Cut

To suppress combinatorial background, a pre-selection cut is applied on the variable:

$$\Delta m_{B_s^0} = m^{\text{rec}}_{B_s^0} - m^{\text{rec}}_{\tau^+} - m^{\text{rec}}_{\tau^-} \tag{2}$$

where m^{rec} refers to the reconstructed invariant mass of the visible systems (6π for B_s^0 and 3π for each τ). A rectangular cut is applied at 900 MeV/c^2, as shown in Fig. 5.

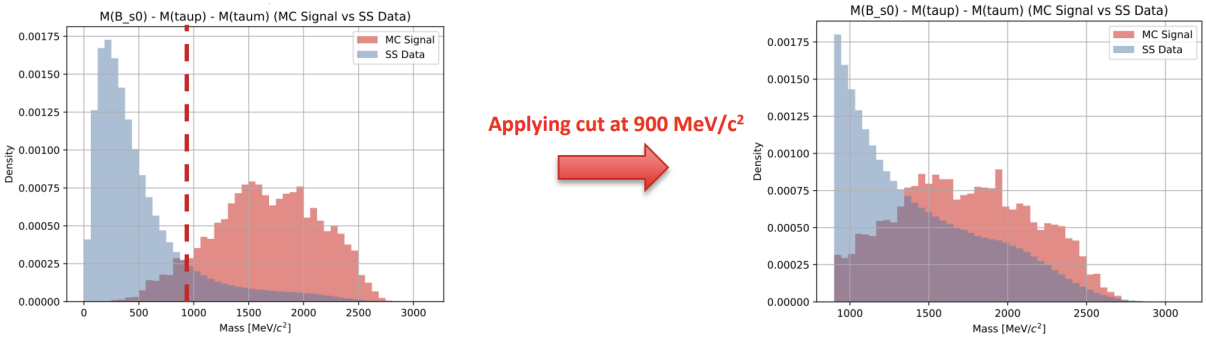

Figure 5: Distribution of $\Delta m_{B_s^0}$ for MC Signal (red) and SS Data (blue), before (left) and after (right) the cut applied at 900 MeV/c^2. The signal is retained in the higher mass region while the background, which dominates low Δm, is heavily suppressed.

As shown in Tab. 3, this cut retains 92.52% of the signal while rejecting over 85% of the combinatorial background.

Table 3: Efficiencies of the $\Delta m_{B_s^0}$ cut.

Sample	Events Before	Events After	Efficiency
MC Signal	4,772	4,415	92.52%
SS Data (Comb. Bkg)	8,481,222	1,234,561	14.56%
OS Data	12,963,547	1,791,389	13.82%

3.2 BDT

A Boosted Decision Tree (BDT), specifically using the XGBoost algorithm [10], is trained to further separate signal from combinatorial background. BDTs are effective in HEP for exploiting non-linear correlations between multiple discriminating variables to build a strong classifier.

3.2.1 BDT Variables

The input features characterize the geometry, kinematics, and isolation of the decay.

- **Kinematic Variables:**
  - `pv_tau_angle_deg`: The angle θ (in degrees) between the vectors from the primary vertex (PV) to end vertices of the two τ candidates (TV):

$$\theta = \arccos\left(\frac{\vec{v}_{\tau+} \cdot \vec{v}_{\tau-}}{|\vec{v}_{\tau+}||\vec{v}_{\tau-}|}\right) \times \frac{180}{\pi} \tag{3}$$

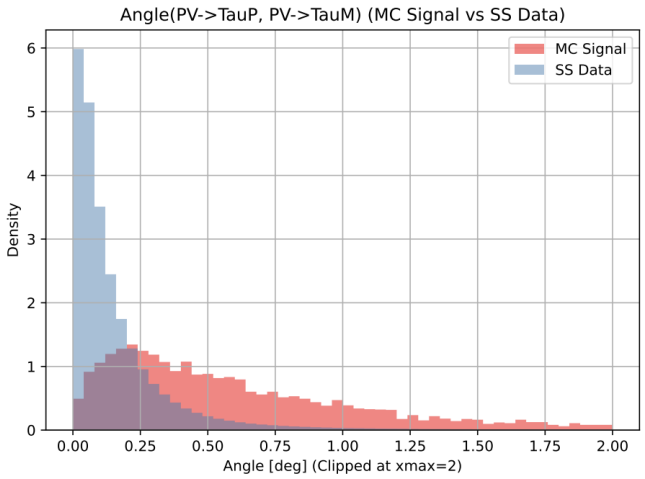

Figure 6: Background events (blue) peak sharply at low angles, indicating the reconstructed momenta for signal events (red) do not align as well with the flight path as the background.

– `min_log10_one_minus_OWNPV_DIRA`: Derived from the DIRection Angle (DIRA), which is the angle between the momentum vector of the particle and the vector connecting the PV to the decay vertex. We use $\min_{\tau^+,\tau^-} \log_{10}(1 - \cos\theta_{\mathrm{DIRA}})$.

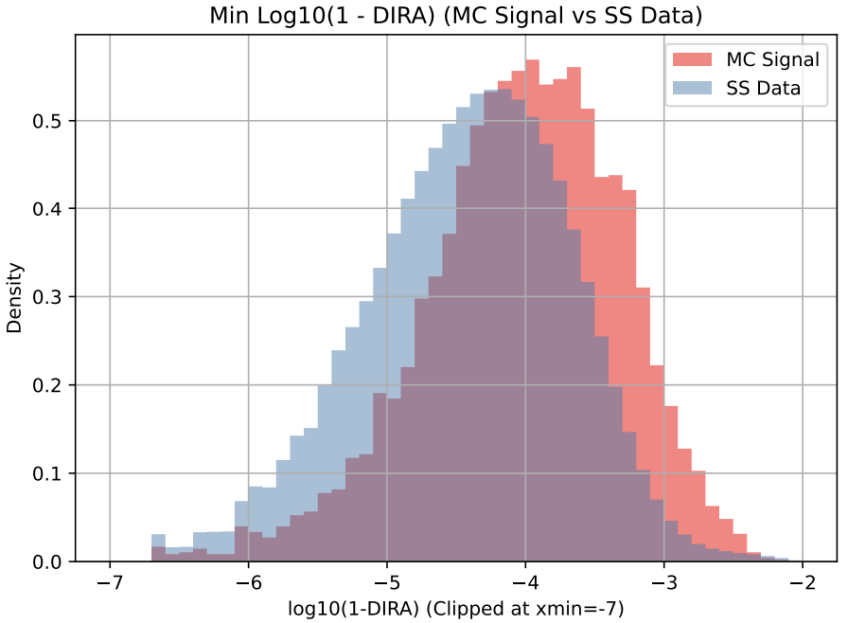

Figure 7: Background (blue) is concentrated at lower values (more negative), corresponding to a DIRA closer to 1 (perfect alignment).

– `taup/taum_three_pi_mass`: Invariant mass $m_{3\pi} = \sqrt{E_{tot}^2 - |\vec{p}_{tot}|^2}$ of the visible pions corresponding to each of the τ candidates.

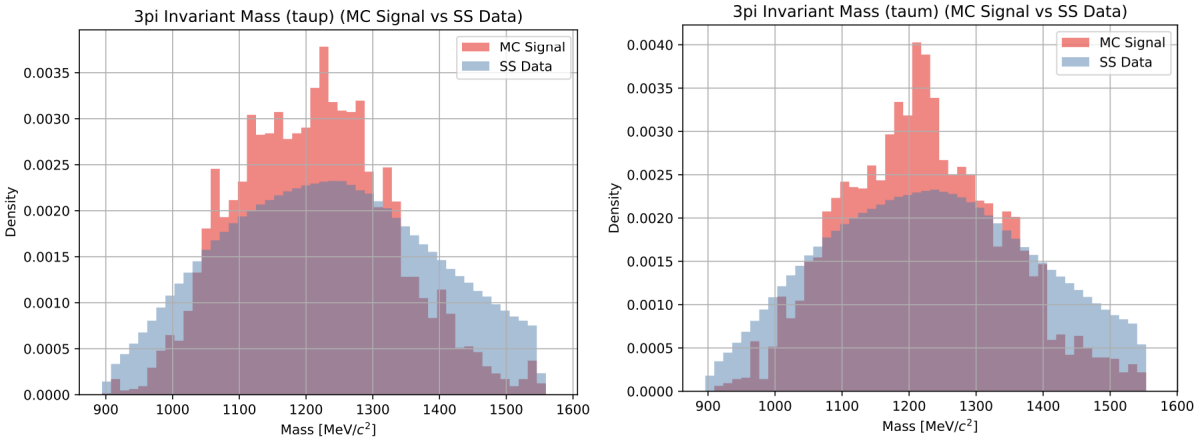

Figure 8: Signal (red) exhibits structure consistent with τ decay kinematics, which decays into $a_1(1260)^-$ and ν_τ, while background (blue) is broader.

– `min_log10_BPV_IPCHI2`: Minimum impact parameter χ^2 between the τ candidates with respect to the PV.

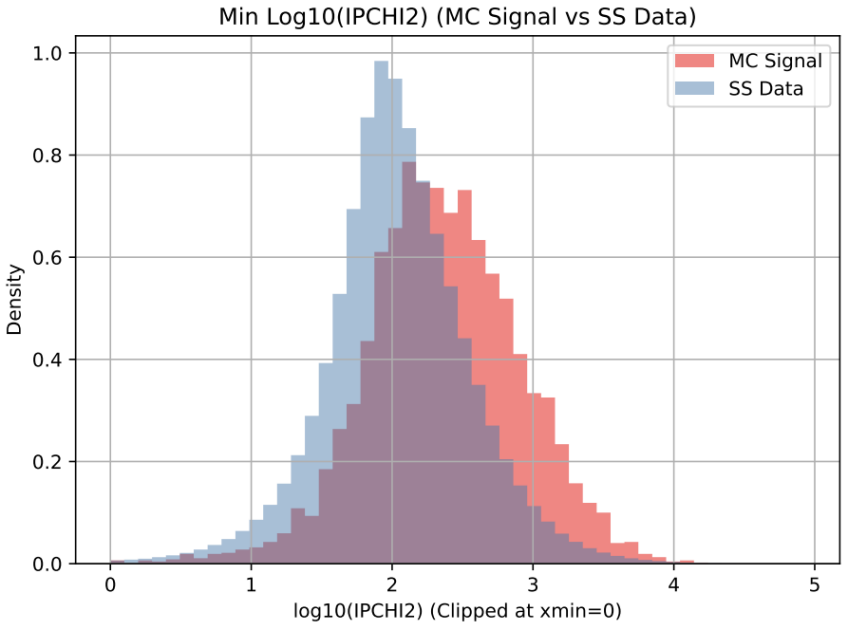

Figure 9: Signal (red) generally has larger IP χ^2 values than background (blue).

– `taup/taum_min_rho_mass_diff`: The minimum mass difference between any pair of pions corresponding to a τ candidate and the ρ meson mass: $\Delta m_\rho = \min_{i,j} |m_{\pi_i\pi_j} - m_\rho|$, where $m_\rho = 775.26$ MeV/c^2.

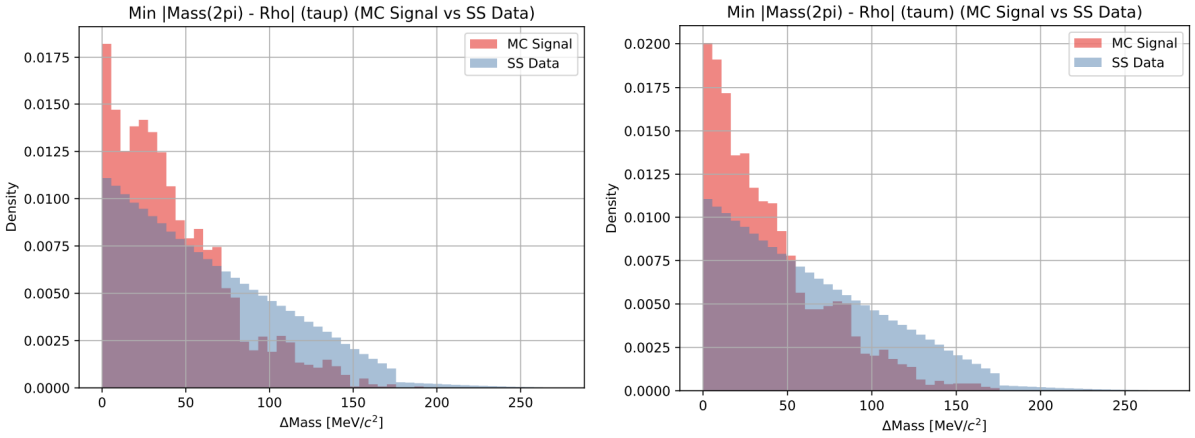

Figure 10: Signal (red) peaks at zero, confirming the resonant decay $\tau \to a_1 \to \rho\pi$, whereas background (blue) is relatively flatter.

– `min_prod_probnn_pi`: Minimum of the product of neural network particle identification probabilities for the three pions corresponding to each of the τ candidate: $\min\{\prod_{i=1}^{3} \texttt{PROBNN\_PI}_{\pi_i(\tau^+)}, \prod_{i=1}^{3} \texttt{PROBNN\_PI}_{\pi_i(\tau^-)}\}$

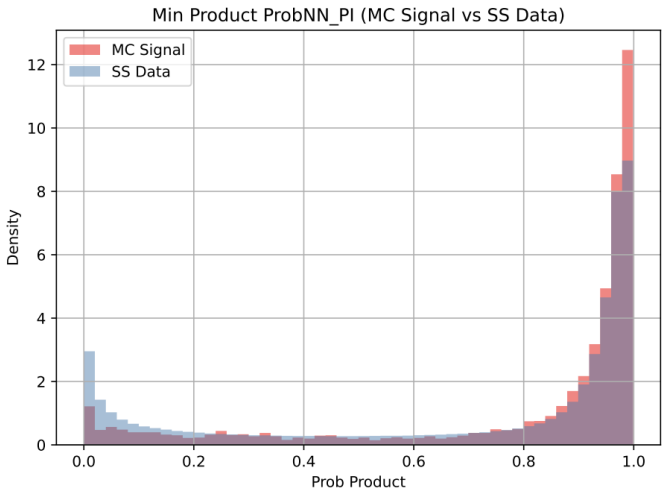

Figure 11: Signal (red) peaks strongly at 1, indicating real pions, while background (blue) contains misidentified particles.

– `tau_end_vertex_distance`: Euclidean distance between the two reconstructed τ decay vertices (TV).

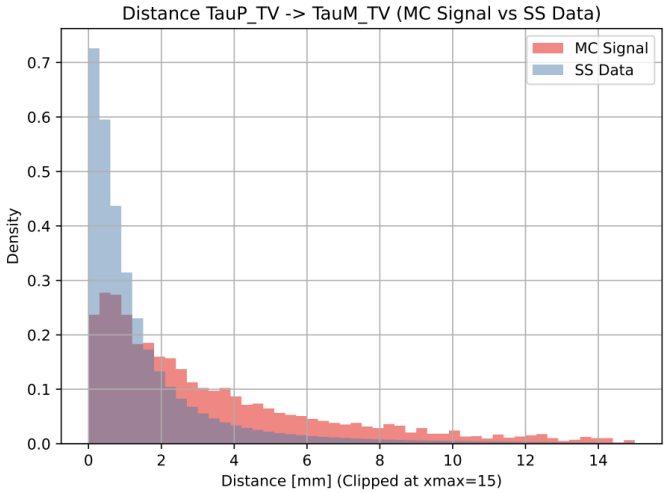

Figure 12: Distance between τ vertices. Combinatorial background (blue) peaks at short distances close to 0, whereas signal (red) distributes flatter with more contribution at larger distances.

- **Isolation Variables:**
  - `B_s0_VTXISO_OneTrack_NParts`: Number of tracks compatible with the B_s^0 vertex reconstruction.

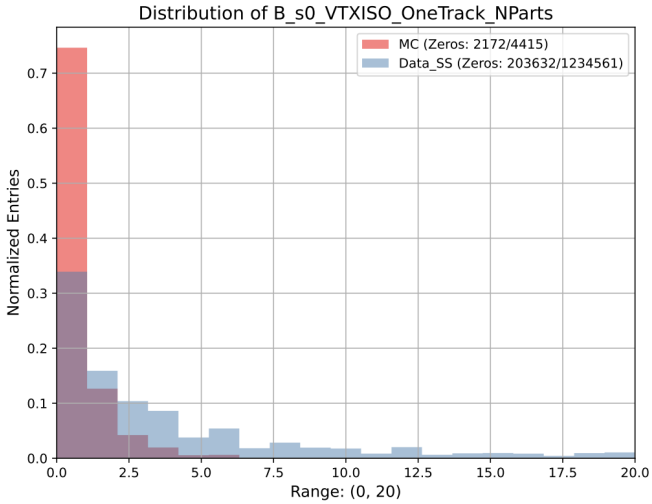

Figure 13: Signal events (red) predominantly have 0 extra tracks (isolated), whereas background (blue) often has additional tracks around the vertex.

  - `B_s0_VTXISO_OneTrack_Smallest_DELTACHI2_MASS`: Mass of the track with smallest $\Delta\chi^2$ added to the PV.

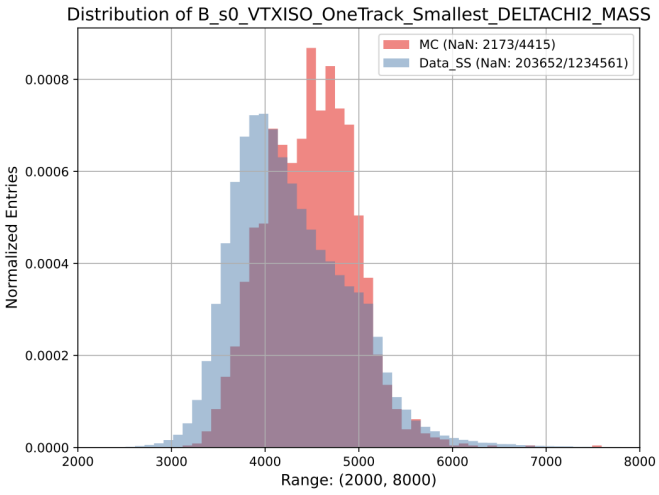

Figure 14: Signal (red) events tend to have larger mass fot the tracks with smallest $\Delta\chi^2$ compared to the combinatorial background (blue).

– `B_s0_HEAD_NC_BIso10_Range_PT`: Difference between the maximum and minimum transverse momentum of the tracks entering the neutral–cone isolation within a radius of 1.0: $p_T^{max} - p_T^{min}$.

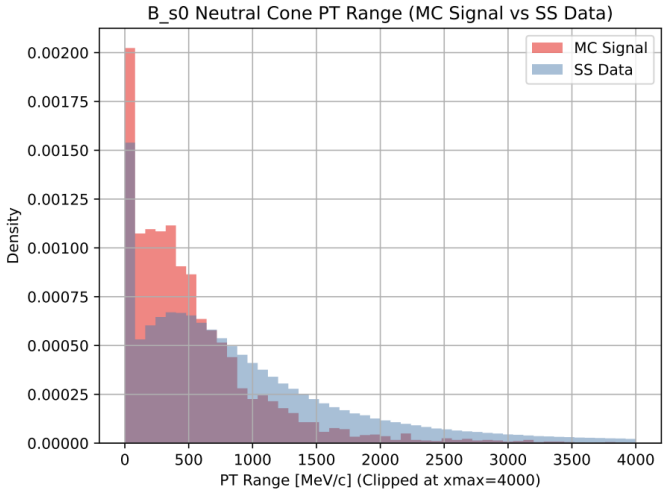

Figure 15: Signal (red) tends towards lower values compared to background (blue). Both distributions show a clear peak at 0.

– `B_s0_HEAD_CC_BIso05_PASY`: Charged-cone asymmetric momentum for the B_s^0 candidate, computed with cone size 0.5: $\frac{p_{head}-p_{cone}}{p_{head}+p_{cone}}$, where p_{head} is the momentum of the candidate inside the head region and p_{cone} is the sum of momenta of particles in the cone used for the isolation.

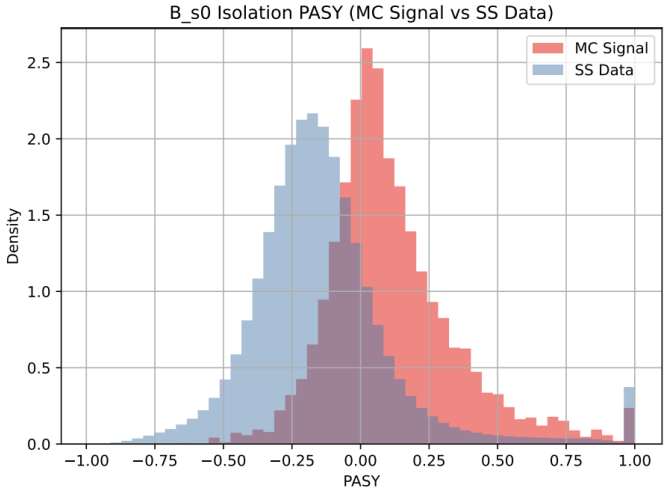

Figure 16: Signal (red) peaks at high values (momentum dominated by the B candidate / cone head), while background (blue) is generally lower.

– `B_s0_VTXISO_OneTrack_Sum_CHI2_DCHI2`: Sum of smallest χ^2 and $\Delta\chi^2$ for tracks added to the vertex reconstruction.

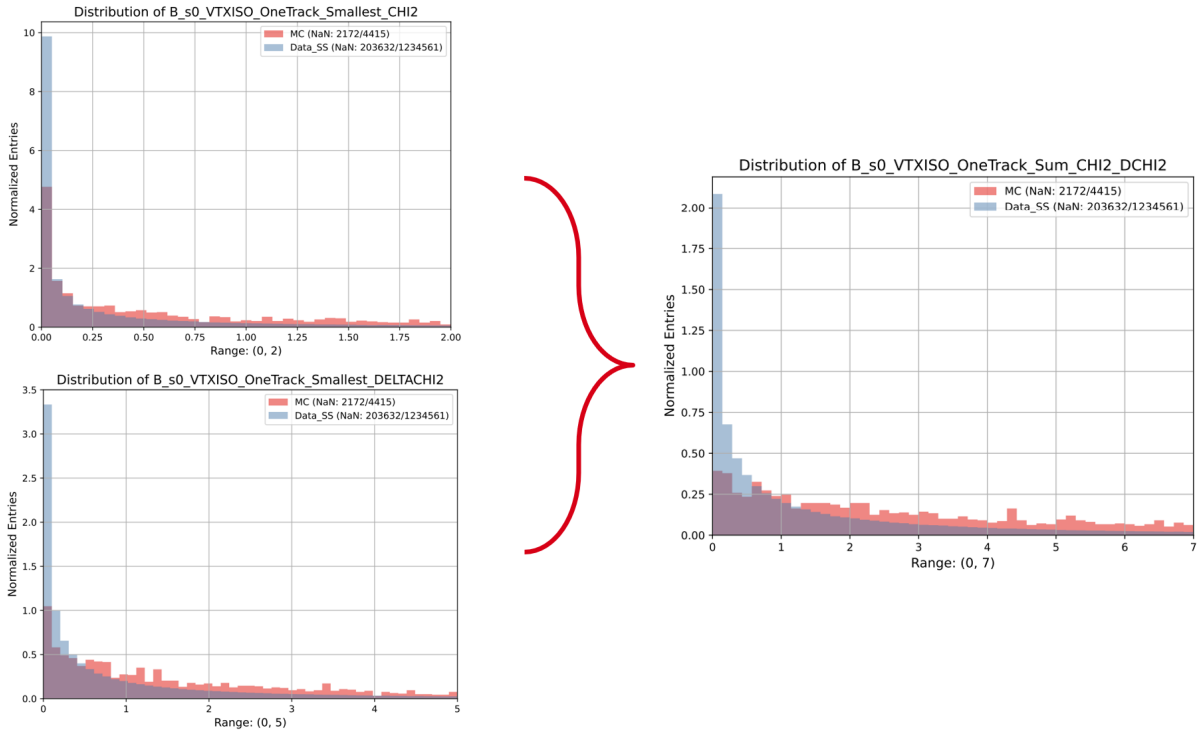

Figure 17: Both smallest χ^2 and smallest $\Delta\chi^2$ distributions show a generally lower value for the SS data. The sum of them shows a stronger discriminating power between Signal (red) and Background (blue).

3.2.2 Changes Compared to Previous Study

1. ρ **Signature Capturing:** The variable

   `taup/taum_min_rho_mass_diff`: $\min_{i,j} |m_{\pi_i\pi_j} - m_\rho|$

   was changed from

   `taup/taum_max_rho_mass_diff`: $\max_{i,j}(m_{\pi_i\pi_j} - m_\rho)$.

   Previously, maximising the difference always selected the pair with the highest mass, which correlates strongly with the total 3π mass. By taking the minimum of the absolute mass difference, we select the pair that is most likely to compose the ρ resonance, effectively capturing this signature of the τ decay.

2. **New isolation variables:** Isolation variables:

   - `B_s0_VTXISO_OneTrack_Smallest_DELTACHI2_MASS`

- `B_s0_VTXISO_OneTrack_Sum_CHI2_DCHI2`

contain NaN values when no tracks are found in the isolation cone (perfect isolation). These were not previously implemented but are now explicitly handled by XGBoost, exploiting the fact that signal events are more likely to be NaN (isolated).

3.2.3 Correlation Matrix

The correlation matrix (Fig. 18) confirms that the new variables, particularly the ρ mass difference, are well dissociated from other kinematic variables. Correlation is observed between DIRA and PROBNN variables, which could be a consequence of them both being measurements of track reconstruction quality.

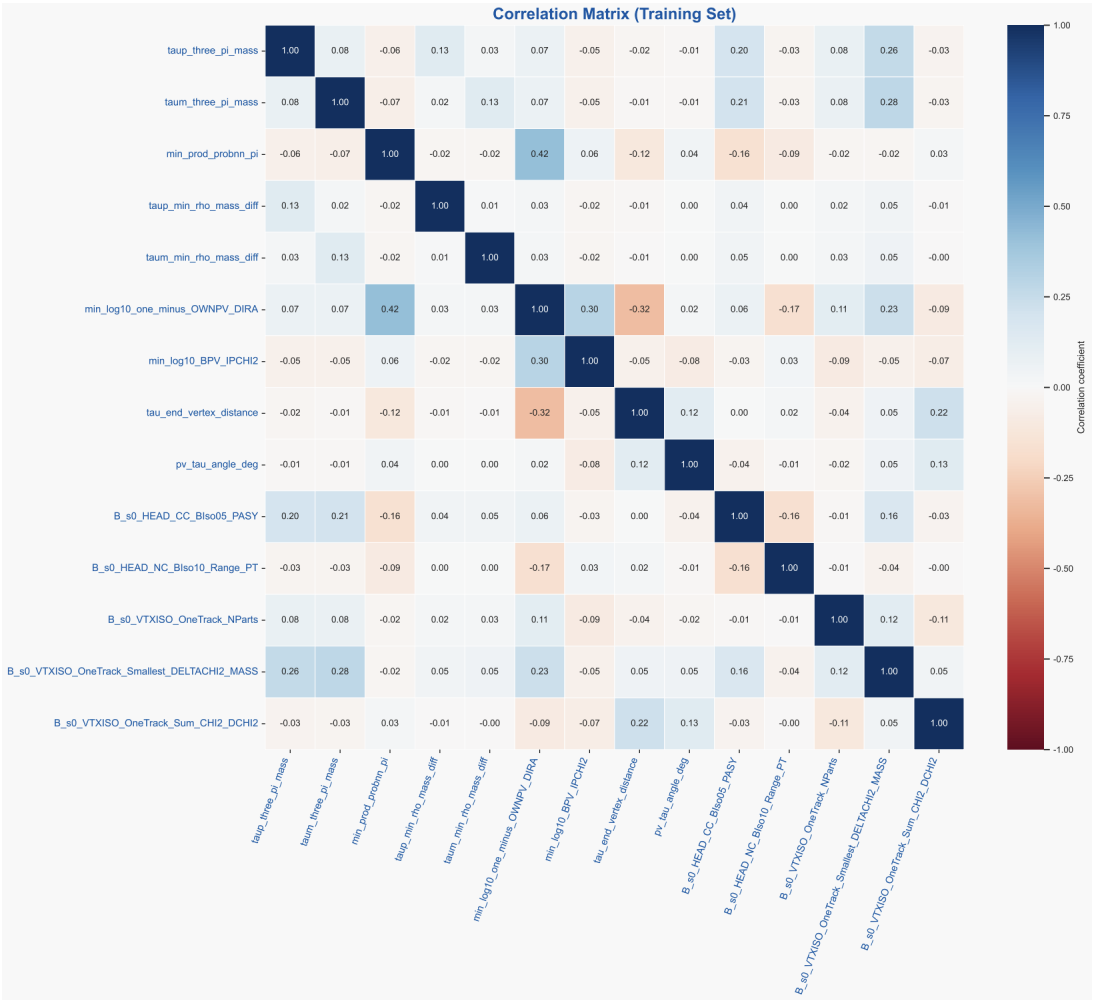

Figure 18: Correlation matrix of the BDT input variables. Overall, good dissociation between variables is achieved.

3.3 Training Parameters and Results

The hyperparameters of the BDT are optimised via Bayesian optimisation method. The optimised parameters are listed in Tab. 4.

Table 4: Optimised XGBoost Hyperparameters.

Parameter	Value
`n_estimators`	150
`max_depth`	3
`min_child_weight`	3
`learning_rate`	0.1425
`subsample`	0.7202
`colsample_bytree`	0.6012
`gamma`	0.4398
`reg_alpha`	0.0037
`reg_lambda`	0.6494

The model achieved a **Test AUC of 0.957**, an improvement over the previous result of 0.932. Fig. 19 shows the ROC curve and the output distribution, indicating good signal-background separation and no significant overtraining.

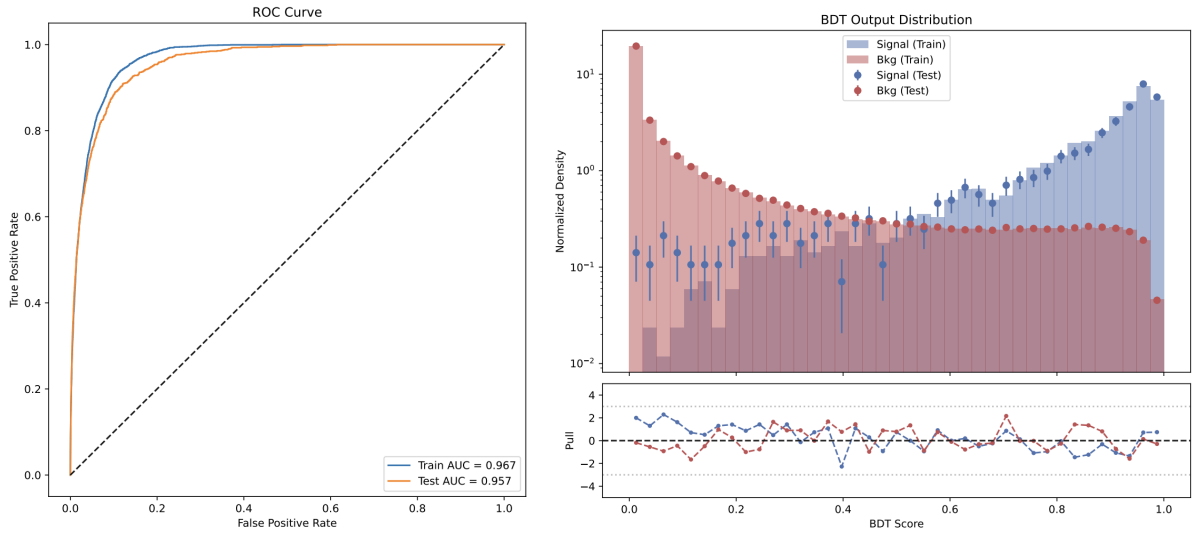

Figure 19: Left: ROC Curve. Right: BDT Output Distribution showing separation between Signal (blue) and Background (red). The small overtaining gap is a result of low statistics at lower end of the signal sample.

3.3.1 SHAP Value and Feature Importance

SHAP (SHapley Additive exPlanations) values were used to interpret the model [11], as shown in Fig. 20. The plot effectively indicates the correlation between the numerical value of a variable (colour code) and its impact on the final output (lower SHAP value → less likely to be a signal).

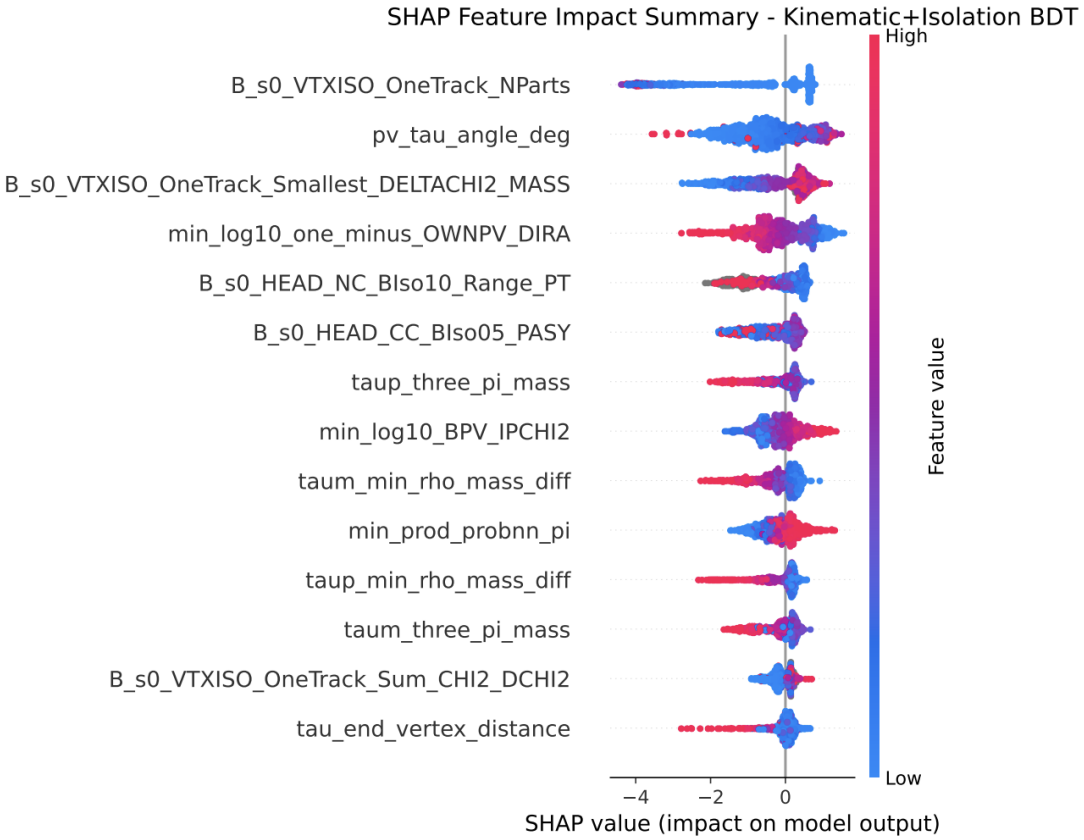

Figure 20: SHAP value plot provides an intuitive way to visualise how numerical values of a BDT feature impacts the final output of the model.

The mean of absolute SHAP values for each variable can be used as an indication of their relative importance when training the model, as shown in Fig. 21. This plot identifies `B_s0_VTXISO_OneTrack_NParts` as the most impactful feature, confirming that vertex isolation is the strongest discriminator against combinatorial background.

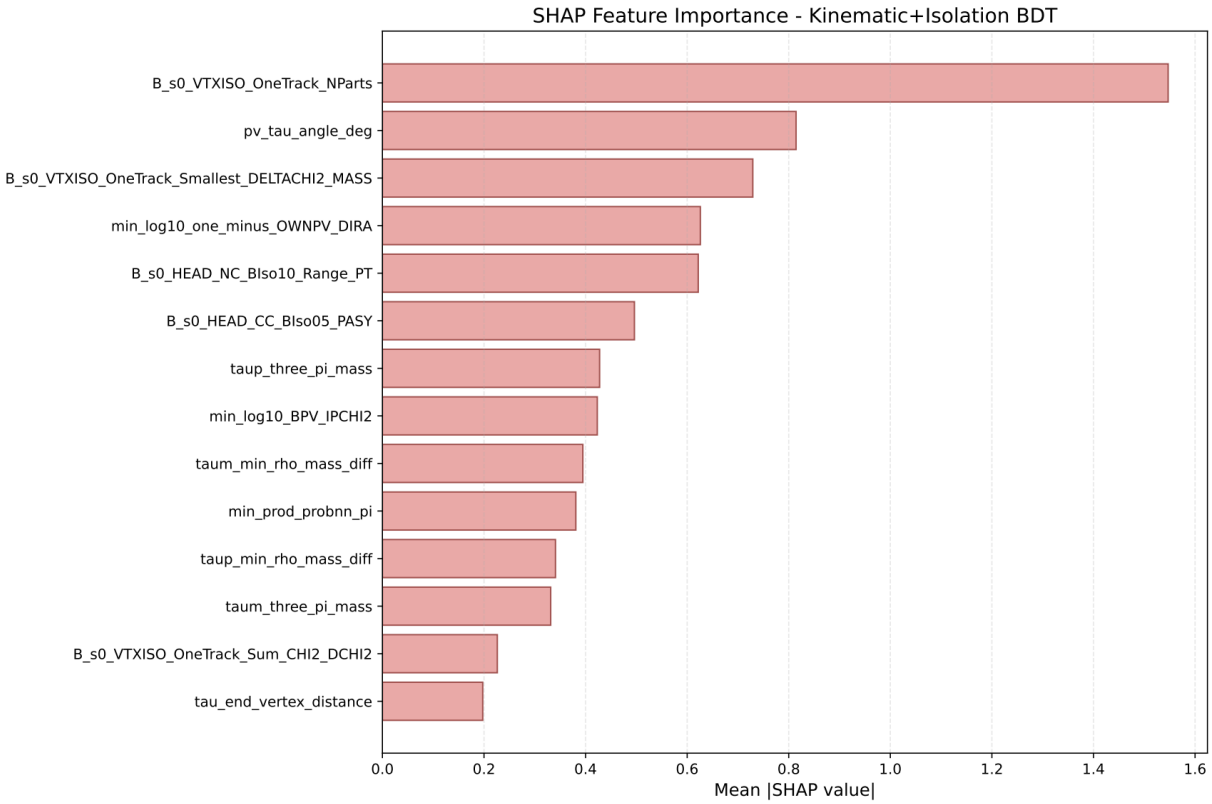

Figure 21: SHAP Feature Importance ranking variables by mean impact.

3.4 BDT Thresholds

To evaluate the total performance, we combine the BDT efficiency with the efficiency of the initial $\Delta m_{B_s^0}$ cut, which serves as a baseline (Tab. 5).

Table 5: Efficiency of the pre-selection $\Delta m_{B_s^0}$ cut.

MC Signal Eff.	SS Data Eff.
92.52%	13.82%

The overall efficiencies (including the pre-cut) for various BDT thresholds are presented in Tab. 6.

For the purpose of this study, a BDT threshold of 0.8230 is chosen as the reference for this selection, where an overall SS Data efficiency of 0.46% is reached (improved from 0.70% of the previous study) while maintaining 60.00% of the MC Signal events.

Table 6: Overall Efficiencies (including Δm cut) at different BDT thresholds.

BDT Threshold	Overall MC Signal Eff.	Overall SS Data Eff.
0.7290	70.06%	0.74%
0.7820	65.12%	0.58%
0.8230	**60.00%**	**0.46%**
0.8610	55.06%	0.35%
0.8880	50.11%	0.26%

4 Analysis: Physics Background

4.1 Introducing $B^0 \to D^- 3\pi$

We investigated the physics background:

$$B^0 \to (D^- \to \pi^-\pi^+\pi^-\pi^0)\,\pi^+\pi^-\pi^+, \tag{4}$$

which creates a $6\pi + \pi^0$ final state. The missing π^0 mimics the signal's missing energy, and the branching ratio ($\sim 7.0 \times 10^{-5}$) is four orders of magnitude larger than the signal (considering the $\tau \to \pi\pi\pi\nu$ branching ratio).

4.2 Efficiencies Applying Previous Selections

We applied the selection strategy developed for the combinatorial background to this physics background sample. The selection efficiencies are listed in Table 7.

The BDT proves significantly less effective against this topology. While the combinatorial background efficiency was driven down to 0.46%, the physics background efficiency remains at 35.47% after the BDT cut. This outcome confirms that the BDT, having been trained on combinatorial data, does not learn to distinguish the specific kinematic features of the $B^0 \to D^- 3\pi$ decay as it resembles the signal signature to a high extent. Notice that the signal efficiency of 68.19% here, which is higher than the previously mentioned 60.00%, is a result of the BDT being applied to the whole MC Signal sample rather than only the testing sample.

Table 7: Selection efficiencies for Signal vs Physics Background.

Selection Step	**MC Signal**	$\boldsymbol{B^0 \to (D^- \to \pi^-\pi^+\pi^-\pi^0)\,\pi^+\pi^-\pi^+}$
$\Delta m_{B_s^0}$ cut	92.52%	95.81%
$\Delta m_{B_s^0}$ + BDT	68.19%	35.47%

4.3 Kinematic Variable Distributions

To suppress this background, we compared the kinematic distributions of the signal and the B^0 background. Most variables exhibited overlapping profiles, including:

- `taup/taum_three_pi_mass`: The reconstructed visible invariant masses for τ^+ and τ^-.

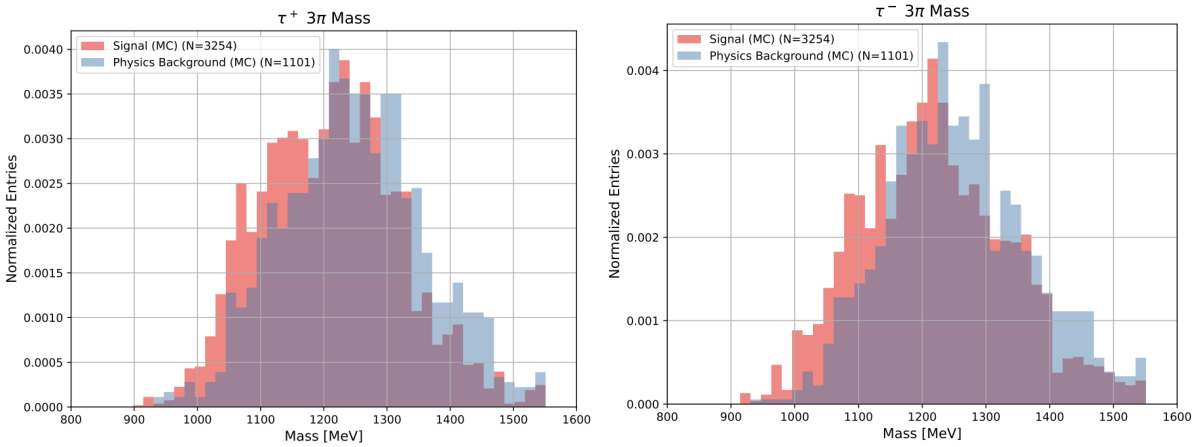

Figure 22: 3π mass for τ^+ (left) and τ^- (right). The physics background tends to exhibit slightly higher 3π masses.

- `PV_TV1/TV2_Distance`: The reconstructed Euclidean distances between the Primary Vertex (PV) and the two Tau Vertices (TV).

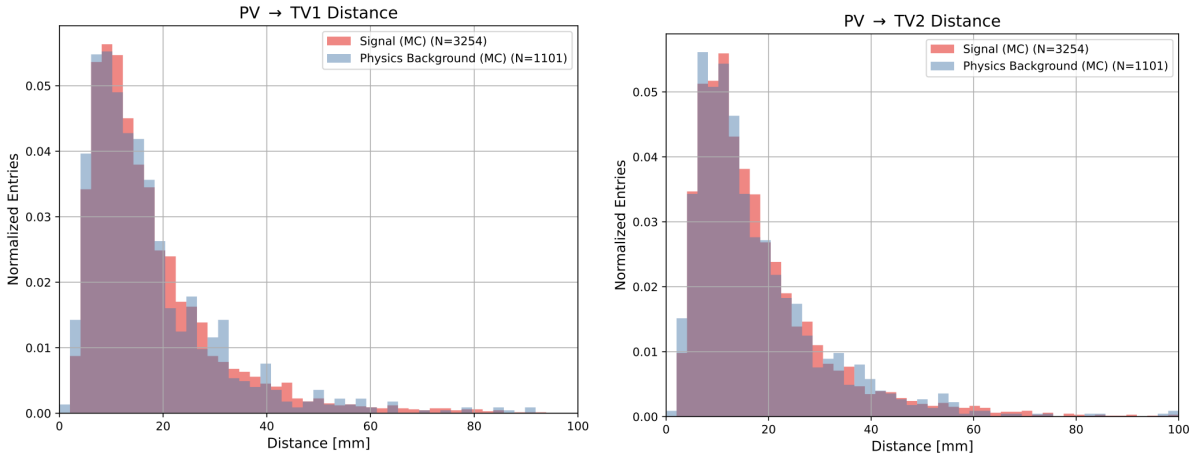

Figure 23: Distance between PV and TV1 (left) and TV2 (right). No significant discrimination power is observed between the signal and background distributions.

- `taup/taum_FD`: Reconstructed flight distances for each τ candidate.

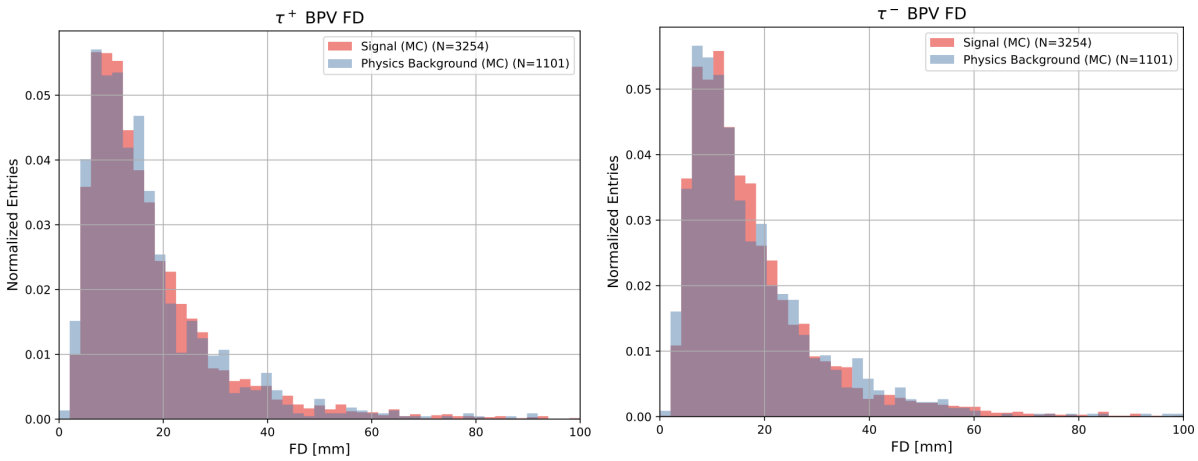

Figure 24: Flight distance of τ^+ (left) and τ^- (right). No obvious difference between the distributions is observed.

- `taup/taum_Lifetime`: Reconstructed lifetimes for each τ candidate.

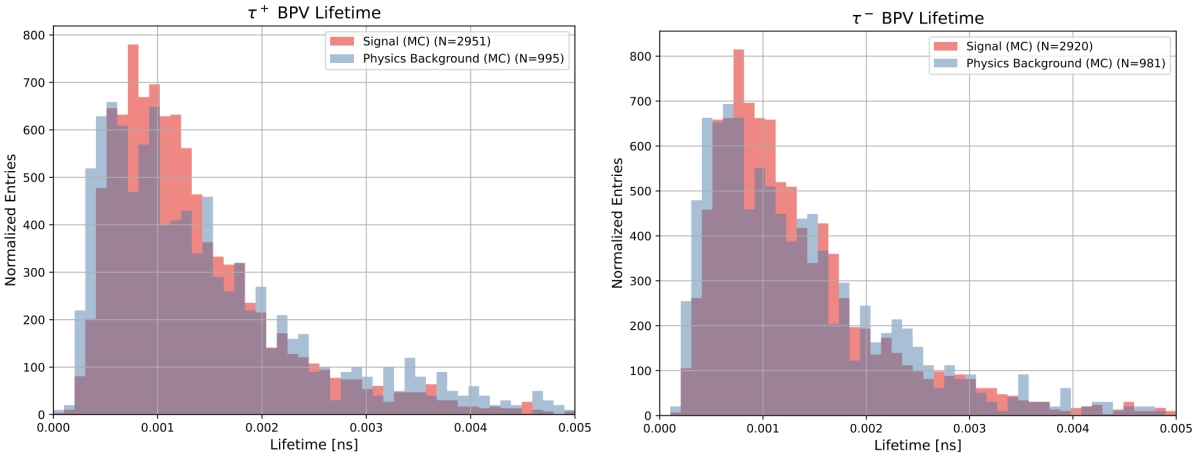

Figure 25: Lifetime of τ^+ (left) and τ^- (right). The physics background (blue) tends to display slightly lower lifetimes.

While minor differences are observable in the variables above, none provide sufficient separation to define a distinct cut. In contrast, a significant distinction was observed in the **6π invariant mass**.

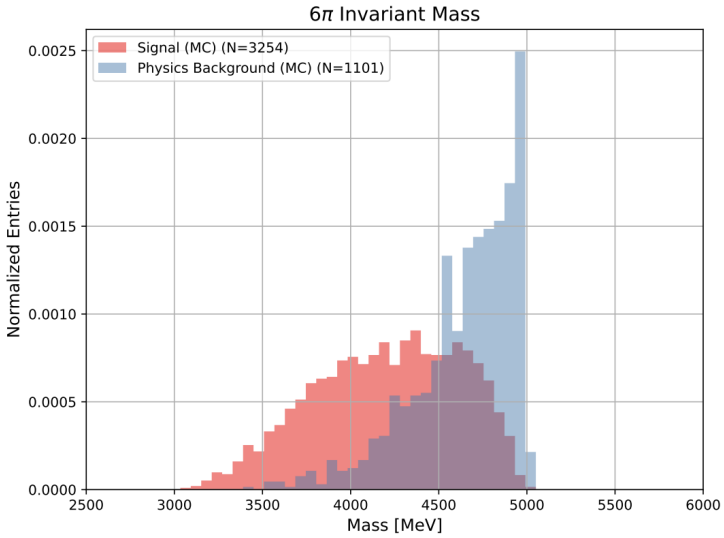

Figure 26: 6π Invariant Mass, showing separation between Signal (red, broad lower mass) and Physics Background (blue, sharp higher mass).

The signal distribution characterises a broad peak centered at lower masses, a consequence of the four missing neutrinos carrying away energy. The background, missing only a single π^0, peaks sharply at a higher mass value, closer to the nominal B^0 mass (5279 MeV/c^2) but shifted down by the π^0 mass. We can therefore apply a rectangular cut to suppress this background.

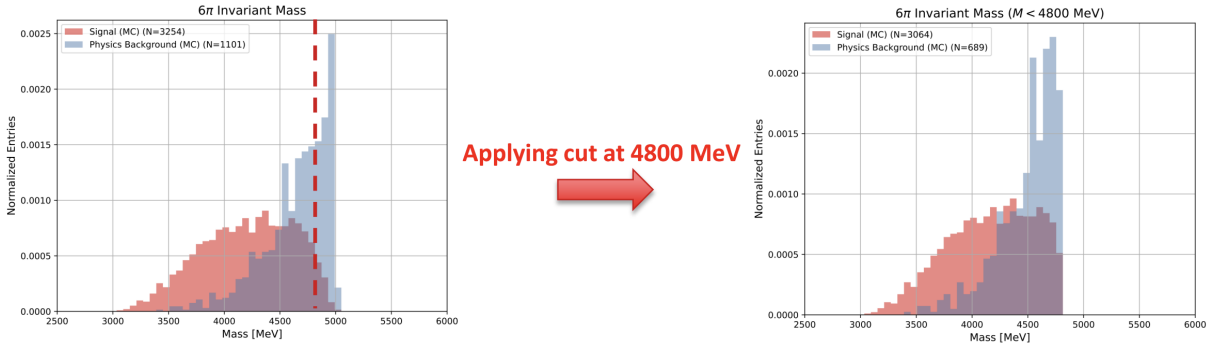

Figure 27: 6π Invariant Mass distribution before (left) and after (right) applying the cut at 4800 MeV. The physics background (blue) is significantly suppressed.

4.4 6π Invariant Mass Cut

Based on the distribution shown in Figure 26, a cut was defined to reject events with high reconstructed mass:

$$M(6\pi) < 4800 \text{ MeV}/c^2 \tag{5}$$

Applying this cut yields the results illustrated in Figure 27 and summarised in Table 8.

The cut is highly effective, providing an overall suppression factor of roughly 5 for the physics background relative to the start. As detailed in Table 8, this cut, along with the previously applied selection strategies, retains 64.21% of the signal relative to the previous step while rejecting a substantial portion of the background.

Table 8: Efficiencies of the $M(6\pi) < 4800$ MeV cut. "Relative" refers to the efficiency of this specific step, while "Total" refers to the cumulative efficiency including $\Delta m_{B_s^0}$ pre-cut and BDT.

Metric	**MC Signal**	$\boldsymbol{B^0 \to (D^- \to \pi^-\pi^+\pi^-\pi^0)\,\pi^+\pi^-\pi^+}$
Relative Efficiency	94.16%	62.58%
Total Efficiency	64.21%	22.20%

5 Conclusion

This report summarised a selection study for $B_s^0 \to \tau^+\tau^-$ search using LHCb Run 3 data.

A BDT selection for combinatorial background suppression has been optimised. By refining the input variables (specifically the ρ signature capturing, as well as inclusion of new isolation variables) and optimising the XGBoost hyperparameters, the model performance is improved to a Test AUC of 0.957. The new selection achieves a combinatorial background efficiency of 0.46% at a signal efficiency of 60.00%, a clear improvement over previous studies.

A preliminary study of the $B^0 \to (D^- \to \pi^-\pi^+\pi^-\pi^0)\,\pi^+\pi^-\pi^+$ physics background is also conducted. Analysis reveals that the combinatorial-trained BDT is not effective against this background (35.47% efficiency), due to the high similarity between its topology and that of the signal. However, the 6π invariant mass variable provides strong discrimination power. A cut at 4800 MeV reduces the physics background overall efficiency to 22.20% while maintaining a signal efficiency of 64.21%.

The expected signal yield in the analysed data sample (Blocks 7 & 8 of 2024) is low (2.26 events), but the full 2024 dataset and upcoming 2025 data with improved triggers will provide the statistics necessary for a more competitive measurement. Future

work should focus on training a dedicated BDT to suppress the physics background and extending the study to other potential background channels such as $B_s^0 \to D_s^+ D_s^-$.

References

[1] Harriet Jarlett. *25 years of Large Hadron Collider experimental programme*. Accessed: 06-11-25. CERN. 2017. URL: https://home.cern/news/news/cern/25-years-large-hadron-collider-experimental-programme.

[2] LHCb Collaboration. *LHCb Tracker Upgrade Technical Design Report*. Tech. rep. 2014. DOI: 10.17181/CERN.OOOE.909T. URL: https://cds.cern.ch/record/1647400.

[3] P. Alvarez Cartelle et al. "Luminosity measurement with the LHCb RICH detectors in Run 3". In: *JINST* 20.08 (2025), P08001. DOI: 10.1088/1748-0221/20/08/P08001.

[4] R. Aaij et al. "Allen: A High-Level Trigger on GPUs for LHCb". In: *Comput. Softw. Big Sci.* 4.1 (2020), p. 7. DOI: 10.1007/s41781-020-00039-7.

[5] Federica Oliva. "Performance of LHCb Upgrade I in Run 3". In: *20th International Conference on B-Physics at Frontier Machines*. Vol. BEAUTY2023. PoS. 2024, p. 035. DOI: 10.22323/1.443.0035.

[6] Christoph Bobeth et al. "$B_{s,d} \to l^+l^-$ in the Standard Model with Reduced Theoretical Uncertainty". In: *Phys. Rev. Lett.* 112 (2014), p. 101801. DOI: 10.1103/PhysRevLett.112.101801.

[7] Roel Aaij et al. "Search for the decays $B_s^0 \to \tau^+\tau^-$ and $B^0 \to \tau^+\tau^-$". In: *Phys. Rev. Lett.* 118.25 (2017), p. 251802. DOI: 10.1103/PhysRevLett.118.251802. arXiv: 1703.02508 [hep-ex].

[8] R. Aaij et al. "Measurement of the b-Quark Production Cross Section in 7 and 13 TeV pp Collisions". In: *Phys. Rev. Lett.* 118 (5 Feb. 2017), p. 052002. DOI: 10.1103/PhysRevLett.118.052002. URL: https://link.aps.org/doi/10.1103/PhysRevLett.118.052002.

[9] Jhovanny Mejia. "Investigating Bottom Quark Energy Loss, Hadronization, and B Meson Nuclear Modification Factors in B^+ and B_s^0 Decays: Insights from CMS in pp, pPb, and PbPb Collisions". In: *EPJ Web Conf.* 316 (2025). Presented at the 21st International Conference on Strangeness in Quark Matter (SQM 2024), p. 04003. DOI: 10.1051/epjconf/202531604003.

[10] Tianqi Chen and Carlos Guestrin. "XGBoost: A Scalable Tree Boosting System". In: *Proceedings of the 22nd ACM SIGKDD International Conference on Knowledge Discovery and Data Mining*. ACM, 2016, pp. 785–794. DOI: 10.1145/2939672.2939785. URL: https://doi.org/10.1145/2939672.2939785.

[11] R. Pezoa, L. Salinas, and C. Torres. "Explainability of High Energy Physics events classification using SHAP". In: *Journal of Physics: Conference Series* 2438.1 (Feb. 2023), p. 012082. DOI: 10.1088/1742-6596/2438/1/012082. URL: https://doi.org/10.1088/1742-6596/2438/1/012082.